Brief Communications

Emergent Properties of the Optic Tectum Revealed by Population Analysis of Direction and Orientation Selectivity

Paul R. Hunter,* Andrew S. Lowe,* Ian D. Thompson, and Martin P. Meyer
MRC Centre for Developmental Neurobiology, King's College London, Guy's Hospital Campus, London SE1 1UL, United Kingdom

How local circuits within the brain process visual information has classically been addressed at the single neuron level. Such reductionist approaches, however, struggle to capture the full scope of functional properties associated with even "simple" brain nuclei. Using population functional calcium imaging, we aim to describe how local circuits within the zebrafish optic tectum process visual information. Specifically, how are previously identified direction-selective (DS) and orientation-selective (OS) retinal ganglion cell (RGC) inputs (Nikolaou et al., 2012) represented in tectal cells? First, we identify an emergent population of DS tectal cell with a direction preference not explicitly present in any one of the RGC inputs. Second, this is associated with a striking shift from a tiled and triangular representation of directional space (RGC inputs) into an overlapping cardinal representation by tectal cell populations. Third, and in contrast, we find that orientation space is represented similarly in both the RGC input and tectal cell populations illustrating feature-dependent differences in how tectal circuits process their inputs. Finally, we identify OS and two populations of DS cells at the superficial border of the tectal neuropil, one of which is an emergent population. This study, together with our previous one (Nikolaou et al., 2012), demonstrate that direction-selectivity is established in both the retina and tectum.

Introduction

In many areas of the brain devoted to sensory processing, local circuits transform their inputs to generate a novel representation of the external world. Such emergent properties reflect local circuit computations, with direction- and orientation-selectivity in primary visual cortex often cited as classic examples of emergence (Hubel and Wiesel, 1962; Priebe and Ferster, 2012). Correctly identifying a given output of a local circuit as an emergent property requires certainty that it is not a feature of the local inputs. Strategies that describe the populations of inputs and outputs associated with a local circuit (Carandini, 2012) enable the inference that the circuit generates the emergent property.

Here we adopt a population-based approach to identify computations performed by the zebrafish optic tectum. The tectum is a primary target of retinal ganglion cell (RGC) axons and serves to transform visual information into motor commands that orient the head and body. We have recently provided a description of how the population of RGC inputs into the tectum encode the direction of motion of a drifting bar stimulus (Nikolaou et al., 2012). Here we address how the population of postsynaptic tectal neurons respond to the same stimulus, identifying emergent properties of tectal circuits from the functional differences between the input and output populations.

We find that both direction-selective (DS) and orientation-selective (OS) tectal cells occur in two spatially distinct domains: the cell body region of stratum periventriculare (SPV), the periventricular neurons (PVNs), and a superficial layer of cells that likely consist of inhibitory interneurons (superficial interneurons, SINs; Del Bene et al., 2010). We identify a class of DS-PVN and a class of DS superficial cell with direction preferences not explicitly present in any one of the RGC inputs. The emergent population of DS-PVNs is coupled with a shift from a tiled and triangular representation of directional space by three DS subtypes of RGCs into an overlapping cardinal representation by four DS-PVN populations. In contrast, we find that orientation space is represented similarly in both the RGC input and tectal cell populations. These findings demonstrate that in zebrafish, direction- and orientation-selectivity are inherited from the retina and that DS responses can also be generated *de novo* in the tectum.

Materials and Methods

Animals. Zebrafish were maintained at 28.5°C on a 14 h ON/10 h OFF light cycle. Transgenic lines used: *Tg*(*Isl2b:Gal4*; Ben Fredj et al., 2010), *Tg*(*UAS:tagRFP*; a gift from Chi-Bin Chien, Department of Neurobiology and Anatomy, University of Utah, Salt Lake City, UT), *Tg*(*UAS:SyGCaMP3*; Nikolaou et al., 2012), and *Tg*(*elavl3:GCaMP5*; Ahrens et al., 2013). All experiments were performed in the pigmentation mutant, *nacre* which lacks skin melanophores (Lister et al., 1999). Larvae were too young to determine sex; the dataset therefore includes a mix of males and females. This work was approved by the local Animal Care and Use

Received April 8, 2013; revised June 27, 2013; accepted July 4, 2013.

Author contributions: P.R.H., A.S.L., and M.P.M. designed research; P.R.H. performed research; P.R.H. and A.S.L. contributed unpublished reagents/analytic tools; P.R.H. and A.S.L. analyzed data; P.R.H., A.S.L., I.D.T., and M.P.M. wrote the paper.

P.R.H. and M.P.M. were supported by MRC project grants and a Career Development Award awarded to M.P.M. (G0801242, G1100162, G0600107). A.S.L. and I.D.T. were supported by a Wellcome Trust program grant awarded to I.D.T. (083205). We thank Samuel Barnes, Nikolas Nikolaou, Alison Walker, Fatima Abbas, and Kathleen Dolan for comments on the paper and Jennifer Li, Drew Robson, Florian Engert, and Alex Schier for providing the *Tg(elavl3:GCaMP5)* line.

*P.R.H. and A.S.L. contributed equally to this work.

The authors declare no competing financial interests.

Correspondence should be addressed to Dr. Martin Meyer, MRC Centre for Developmental Neurobiology, King's College London, Guy's Hospital Campus, London SE1 1UL, UK. E-mail: martin.meyer@kcl.ac.uk.

DOI:10.1523/JNEUROSCI.1493-13.2013

 0270-6474/13/3313940-06$15.00/0

Committee, King's College London, and was performed in accordance with the Animals (Experimental Procedures) Act, 1986, under license from the United Kingdom Home Office.

OGB injections, imaging, and analysis. Oregon Green 488 BAPTA-1, AM (OGB; Invitrogen Life Technologies) bolus injections were performed as previously described (Niell and Smith, 2005). Two hours postinjection, larvae were immobilized in 2% agarose and mounted inside a custom-made imaging chamber. Imaging and voxelwise analysis were performed as described previously (Nikolaou et al., 2012). Visual stimuli consisted of dark bars (8 cd/m2) on a mean gray background (32 cd/m2). Each bar was 10° in width, moving at 20°/s, separated from the preceding bar by 30°, enabling more than one bar on the screen at any one time. The long axis of the bar was orthogonal to the direction of motion.

Drug treatments. APV (50 μM) and NBQX (10 μM) were pressure-injected into one tectal hemisphere of *Tg*(*elavl3:GCaMP5*) larvae. Fish were imaged immediately postinjection. Animals were only included if visual responses were not detected in tectal cell soma following treatment.

Identification of DS and OS cells. DS responses were identified using vector sum analysis (Swindale, 1998) with an empirically derived vector sum magnitude threshold (>0.001). A calculation of a normalized vector sum was precluded because of occasional negative integral values as a result of asymmetric jitter around the baseline, hence the absolute vector sum values derived in this study. The absolute values associated with our vector sum reflect the small signal changes rather than the degree of direction-selectivity. To determine OS responses, a multiparametric definition was used: OS index (OSI >0.5) and 1-circular variance (<0.4; Fig. 1*Dii*; Batschelet, 1981; Niell and Stryker, 2008). For automatic cell-segmentation, DS- or OS-defined voxels were spatially aggregated into islands of like responses whose spatial extent was 15–70 voxels (~7–31 μm^{2-} the approximate size limits of a cell soma at this age). The center-of-mass of each aggregation was labeled with the median vector sum angle (DS) or median complex angle (OS) of all constituent voxels. To ensure each aggregation represented a response from a single cell, the variance of preferred angles was examined and those with large variance that suggest mixed responses from more than one cell were excluded (~0.8% of aggregations were excluded due to variances > ±5°).

Alignment of parametric maps to standard space. Parametric maps represent the spatial distributions of either DS or OS responses within individual fish (six maps per fish, three imaging planes with DS and OS maps per plane). The center-of-mass of each voxel aggregation described above was used to summarize cell positions. Anatomical images (mean image of the functional imaging data) were determined for each fish and registered (rigid body: spm8 http://www.fil.ion.ucl.ac.uk/spm/software/spm8) to a "template" fish, expressing the red fluorescent protein, tagRFP, in RGC axons and with OGB-labeled tectal cells. Registration transformations were applied to the individual parametric maps. This standard space allowed composite maps of the tectal data to be generated.

Spatial segregation of PVNs and superficial neuropil cells was achieved by applying two 3-D inclusion masks. The first mask consisted of a smoothed, thresholded image of the RGC axons. OGB-labeled cells within this mask were considered superficial neuropil cells. The second mask was generated by delineation of the PVN region using anatomical borders in the OGB-labeled template tectum. OGB-labeled cells within this mask were considered PVNs.

Determining DS and OS subtypes. To derive the number of subtypes of DS or OS tectal cell within each class, cumulative histograms summarizing the incidence of cells over binned preferred angles (0–360° for DS; 0–180° for OS responses) were generated (Figs. 2,3, and 4, respectively). Multiple von Mises distributions were summed (1–4 depending on the class and location of tectal cells) and fitted to the cumulative histograms using a multidimensional constrained nonlinear minimization approach, with peak-center, height, concentration, and base height being free dimensions. In all cases, the residuals of the fitted summed distributions were inspected for missed coherent populations. For the DS-PVN cumulative histograms, four individual distributions were summed (initially three RGC populations plus one evident residual population); superficial DS cells were fitted with two distributions (two evident populations), the superficial OS cells, with no obvious distinct populations were attempted with one distribution but failed. The OS-PVN cumulative histogram was fit by four distributions (four RGC populations determined by a wavelet decomposition and cluster analysis approach; Lowe et al., 2013); no coherent residuals remained.

Populations of each subtype of response were determined by band-limiting responsive cells to those within 2× the bandwidth of each fitted von Mises-derived population peak (±1.5× bandwidth for OS populations). Separation of populations was statistically compared using a Welch's *t* test using parameters (peak-center and concentration) derived from the fitted von Mises distributions for each subtype.

Results

Functional imaging and parametric mapping of tectal cells

Functional imaging of tectal cells labeled with the fluorescent calcium indicator OGB in 7 d postfertilization (dpf) zebrafish larvae enabled a large-scale analysis of motion-sensitive responses. At 7 dpf, retinotectal synapse density has reached a plateau (Niell et al., 2004; Meyer and Smith, 2006). Moving dark bars were presented in 12 pseudo-randomly ordered orientations while performing confocal imaging of the labeled tectum (Fig. 1*A*,*B*). Metrics were applied to all visually responsive voxels within each experiment ($n = 60$) to define those that exhibited DS or OS responses, before automatic aggregation of voxels into cell body-sized units (see Materials and Methods).

The preferred angles and spatial distribution of DS or OS cells in a single tectum are shown in Figure 1*C*. A 3-D composite stack of all DS and OS tectal cells from all experiments, along with tagRFP-labeled RGC axons, shows that DS and OS tectal cells are located in the PVN region (Fig. 1*D*, white arrowheads) and at the superficial surface of the tectal neuropil (Fig. 1*D*, red arrowheads). Given this spatial segregation, DS and OS cells within the PVN region were analyzed separately from those in the superficial neuropil.

Emergent direction-selective properties of tectal circuits

A cumulative histogram of the preferred angles of motion for all DS cells within the PVN region (DS-PVNs) revealed distinct populations of cells that were fit by four von Mises distributions ($R^2 = 0.89$; Fig. 2*Ai*). The peaks of each von Mises distribution for each population of DS-PVNs are 8°, 89°, 169°, and 261° (Fig. 2*Di*), with dominant populations corresponding to rostrocaudal (RC, ~90°) and caudorostral (CR, ~270°) motion. In comparison, previously reported RGC inputs have three population peaks at 30°, 164°, and 265° (Nikolaou et al., 2012). A direct comparison (Fig. 2*Aii*) of the DS-RGC inputs (red curves) and DS-PVNs (blue curves) illustrates qualitative similarities (three approximately equally spaced populations) and an additional, unique population of DS-PVNs (89°) which represents an emergent property.

To compare the relative proportions of the four DS-PVN populations to the three DS-RGC inputs, populations were normalized to the sum of the three populations that are present in both PVNs and RGCs (Fig. 2*B*). This illustrates that: (1) the relative proportions of the DS subtypes that are present in both the RGCs and PVNs are broadly equivalent, and (2) the tectal population tuned to RC motion represents a substantial additional population.

The tuning properties of the populations of DS-PVNs in relation to the RGC inputs were examined by normalizing responses of each population to the 12 oriented bars to generate polar plots (Fig. 2*C*). Rather than having a single preferred direction, mean response profiles are comparable across a range of directions of motion ("flat-topped"). Both DS-RGC inputs and DS-PVNs entirely fill direction space. Specifically, the three DS-RGC inputs

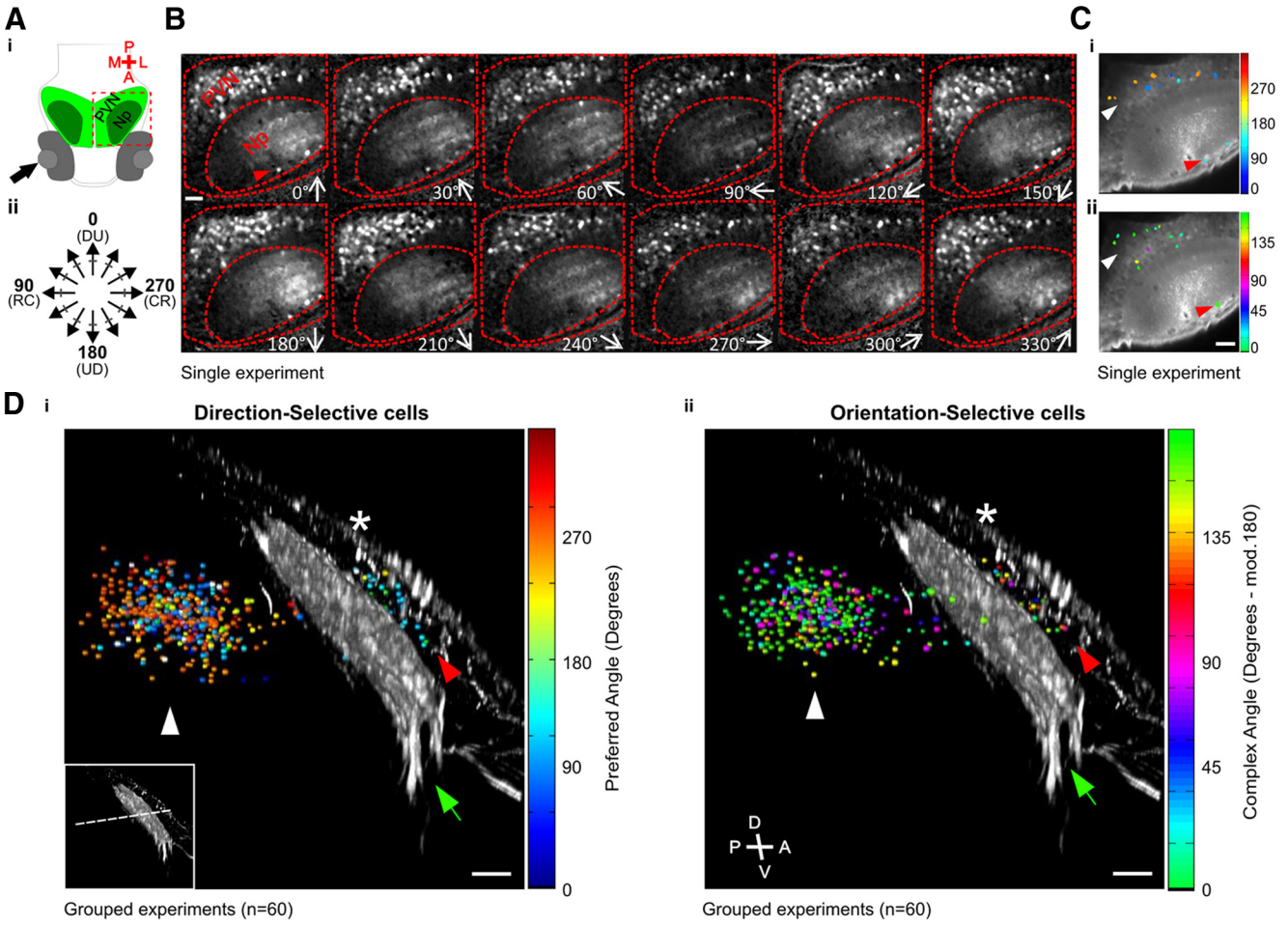

Figure 1. Functional imaging of tectal cells. ***Ai***, Schematic showing dorsal view of zebrafish tectum. Arrow indicates visual stimulation. Np, Tectal neuropil. Red box indicates imaged region. **Aii,**Direction of motion of bars relative to fish body axis. ***B***, Montage showing responses of tectal cells to drifting bar stimulus. Direction of motion is shown bottom right in each panel. Voxel brightness is scaled according to response integral during each stimulus epoch. Red lines show approximate borders of the PVN region and neuropil. Red arrowhead indicates cells at the superficial neuropil. DS (***Ci***) or OS voxel (***Cii***) aggregations overlaid on an OGB fluorescence image of a single tuning experiment, color-coded according to median preferred angle (DS) or median complex angle (OS). White arrowheads, PVNs; red arrowheads, superficial neuropil cells. Color scales to right of images. Sagittal view of DS cells (***Di***) and OS (***Dii***) cells within standard tectal space color-coded as in ***C***. RGC axons labeled with tagRFP (gray). Arrowheads as in ***C***; green arrows, RGC axons; asterisks, skin surface. Approximate functional imaging plane of the experiment in ***B*** is shown as a dashed line in bottom left inset of ***Di***. Scale bar, 20 μm.

appear to tile direction space, whereas the four DS-PVNs have partial overlap between neighboring populations. Interestingly, the three populations of DS-RGC inputs are arranged in triangular organization, whereas the four populations of DS-PVNs display a more cardinal arrangement, suggestive of a shift in the representation of direction-space, rather than an overrepresentation of one segment of direction-space. Opposing populations of DS-PVNs exhibit approximately similar widths of their response profiles. The two almost vertical populations have narrow tuning profiles, mean full-width-half-maximum (±SD) for the 8° population = 64° ± 23°, and 169° population = 49° ± 28° (Welch's *t* test between groups, $p = 0.044$). Conversely, the two almost horizontal populations of DS-PVNs have wider tuning profiles (26° population = 104 ± 28° and 89° = 102 ± 33°; Welch's *t* test between groups, $p = 0.53$) that are more consistent with the CR DS-RGC inputs. Comparisons between all combinations of orthogonal populations (i.e., vertical vs horizontal) demonstrates a statistical difference (Welch's *t* test $p < 0.001$ in all cases) confirming the asymmetric differences in the width of the response profiles between the almost vertical and horizontal DS-PVNs populations.

To rule out the possibility that a population of RGCs tuned to RC motion may have been missed in our previous study (Nikolaou et al., 2012) we reimaged the transgenic line of zebrafish *Tg*(*Isl2b:Gal4;UAS:SyGCaMP3*) at all depths throughout the tectal neuropil. This analysis revealed no additional DS populations to those published previously (data not shown). A population of RGCs tuned to RC motion may also have escaped detection if the Isl2b:Gal4 promoter fails to drive expression in this functional subtype. We therefore analyzed inputs to the tectum using the *Tg*(*elavl3:GCaMP5*) line in which the genetically encoded calcium sensor, GCaMP5, is expressed ubiquitously in the zebrafish brain (Ahrens et al., 2013). Responses of inputs were isolated from tectal dendritic responses by local application of the glutamate receptor antagonists, APV and NBQX. This analysis also did not reveal additional populations of DS input to the tectum (Fig. 2*D*). Collectively these data provide further evidence that the population of RC DS-PVNs is indeed an emergent property of tectal circuitry.

The DS cells within the superficial neuropil region of the tectum represent 23% of the labeled cells in this region (42 DS superficial cells from 180 manually segmented visually re-

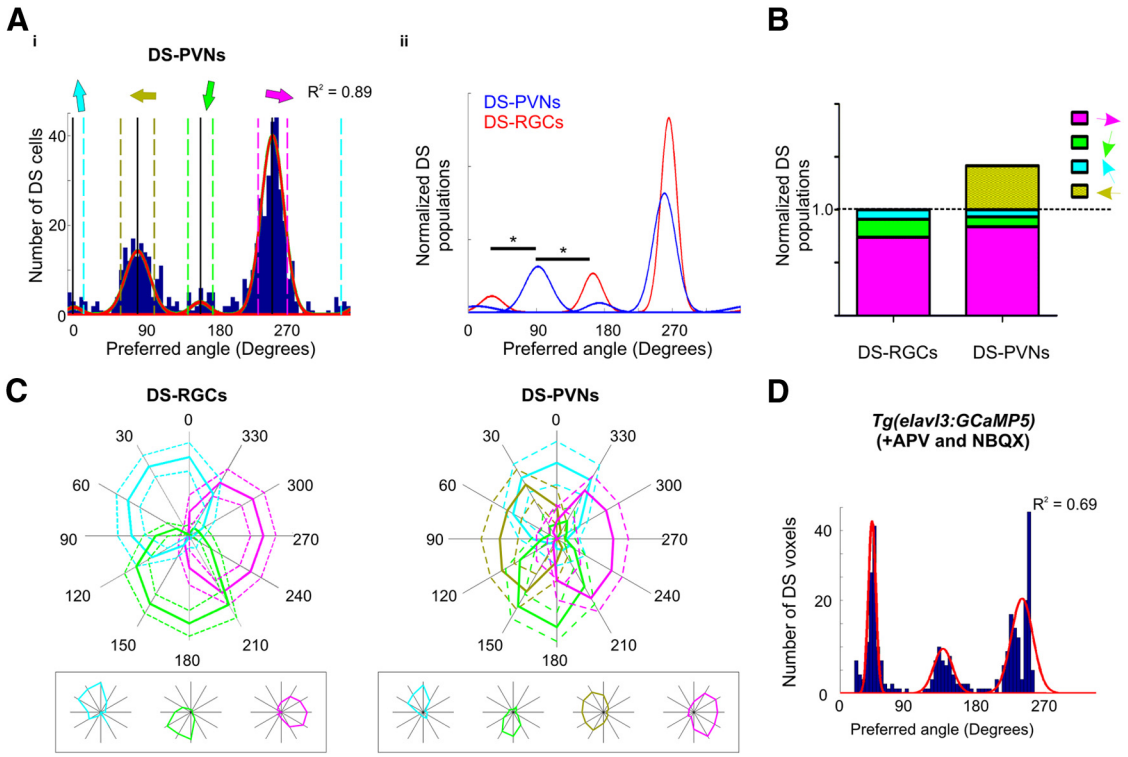

Figure 2. Re-encoding of direction space by periventricular neurons. ***Ai***, Cumulative histogram of summed vector angles for DS-PVNs with four summed von Mises distributions fitted to the data (R^2 value relates to summed von Mises distributions). Colored arrows represent population peaks centers; 8°, 89°, 169°, and 261°. Each population is defined by ±2× bandwidth of each distribution; dashed lines. ***Aii***, Summed distributions of previously identified DS-RGCs (red) and DS-PVNs (blue) populations; areas are normalized to populations tuned to caudorostral motion. Note population tuned to 89°, not present in the RGC population; asterisks, Welch's *t* test, $p < 0.05$. ***B***, Bar chart showing the relative populations of DS-RGC inputs and DS-PVNs color-coded according to population, normalized to the sum of the three populations that are present in both PVNs and RGCs (dashed line). $n = 388$ total number of identified DS-PVNs within all populations. ***C***, Normalized responses of DS-RGCs (left) and DS-PVN (right) populations; mean (solid line) and dashed (±1 SD). Response plots within boxes are single, representative voxels (DS-RGCs) or cells (DS-PVNs) within each population. ***D***, Cumulative histogram of summed vector angles for DS voxels of *Tg*(*elavl3:GCaMP5*) fish treated with 50 μM APV and 10 μM NBQX with three summed von Mises distributions fitted to the data. $n = 7$ fish.

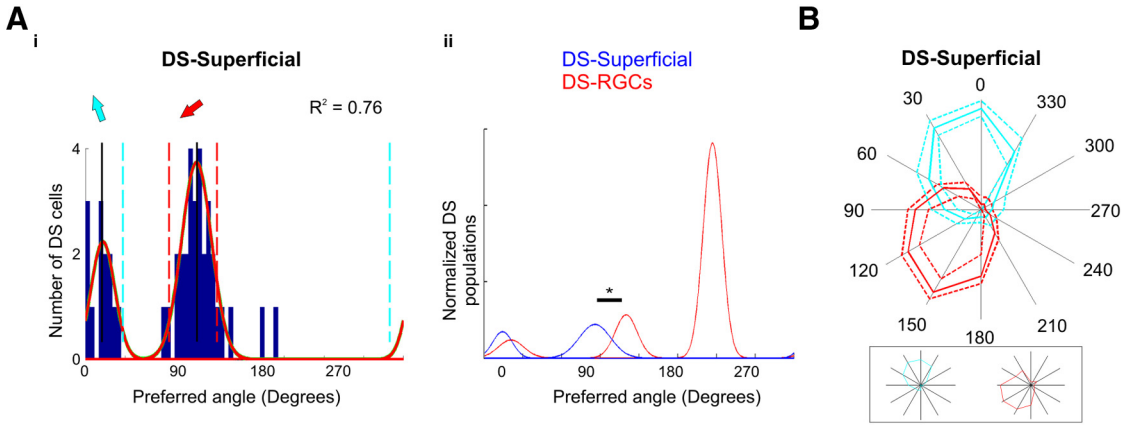

Figure 3. Direction-selective cells at the superficial neuropil. ***Ai***, Cumulative histogram of summed vector angles for DS superficial cells- population peak centers; 21° and 126° (solid red curves). ***Aii***, Summed distributions of previously identified DS-RGCs (red) and DS superficial cells (blue), areas are normalized to the most coherent population. Note population centered at 126° that is not present in the RGC population ; asterisk, Welch's *t* test, $p < 0.05$. ***B***, Normalized responses of the two populations of DS-superficial cells; mean (solid line) and dashed (±1 SD). Response plots within box are single, representative DS superficial cells within each population.

sponsive superficial cells; average of three superficial cells per experiment), compared with 14% DS-PVNs (518 DS-PVNs of 3720 manually segmented visually responsive PVNs; average of 62 responsive PVNs per experiment). Fitting von Mises distributions to the population of superficial DS cells reveals two populations centered at 21° and 126° (Fig. 3*Ai*). Although the preferred angles of the population of superficial tectal neurons centered at 21° overlaps with those of a DS-RGC population centered at 30°, the preferred angles of the population of superficial tectal cells centered ~126° are significantly distinct from those of the any of the DS-RGC inputs (Fig. 3*Aii*, asterisk; Welch's *t* test, $p < 0.05$). This suggests the population of superficial DS neurons centered at 126° represents another emergent population. It should be noted that OGB uptake is

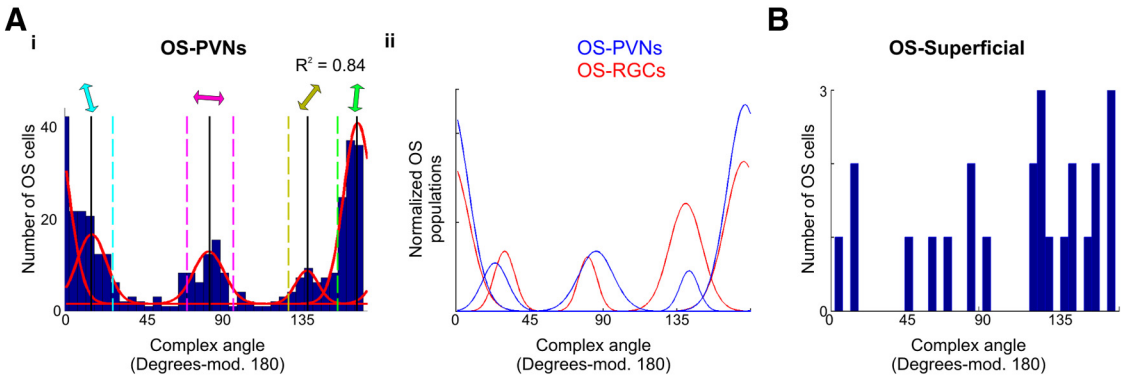

Figure 4. OS-PVN populations. ***Ai***, Cumulative histogram of complex angles for OS-PVNs with four summed von Mises distributions fit to the data (red curves); colored arrows represent populations centered at 16°, 86°, 141°, and 174°. Each population is defined by ±1.5× bandwidth of each distribution; dashed lines. ***Aii***, Summed distribution of previously identified populations of OS-RGCs (red) and OS-PVNs (blue), area normalized to area of all populations. ***B***, Cumulative histogram of preferred complex angles for OS-superficial cells. Scale bar, 20 μm.

widespread in this neuropil region, and thus further populations may have been excluded due to overlapping mixed responses. The tuning profiles of the two identified DS subtypes within superficial neuropil approximately fill the caudal hemisphere of directions of motion (0–180°; Fig. 3*B*).

OS tectal populations are similar to the RGC inputs

OS responses have recently been characterized in the RGC inputs (Nikolaou et al., 2012), and extended in subsequent work that revealed four distinct OS-RGC subtypes (Lowe et al., 2013). We therefore analyzed our functional tectal cell data using the metrics for orientation tuning described above to ask whether coherent populations of OS tectal cells exist.

The cumulative distribution of preferred angles of all identified OS-PVNs is shown in Figure 4*Ai*. Unlike the DS cumulative histograms, OS distributions do not have clearly defined populations. As four populations of OS-RGC inputs have been identified (Lowe et al., 2013) we therefore examined whether four von Mises distributions entirely account for the OS-PVN distributions observed in this study by allowing limited jitter around the preferred angle centers of the OS-RGC inputs. Fitted angle centers of 16°, 86°, 141°, and 174°, with four summed von Mises distributions account for 84% of the data observed in OS-PVNs ($R^2 = 0.84$). Further, no coherent populations of responses were evident within the residuals. Although our approach is not ideal, and may over-fit the four OS-PVNs, it is reasonable to suggest the OS-PVNs mirror the OS-RGC inputs and no emergent OS property is evident (Fig. 4*Aii*). The OS cells within the neuropil region are fewer in number than the DS superficial neuropil cells (Fig. 4*B*; 24 OS cells compared with 43 DS cells). They do not segregate into definable populations based on their preferred complex angles.

Discussion

This study aimed to derive populations of motion-sensitive zebrafish tectal cells to compare with those previously derived for the RGC inputs. We have isolated five populations of DS and four populations of OS tectal cells that can be directly compared with three populations of DS- and four populations of OS-RGC inputs (Nikolaou et al., 2012; Lowe et al., 2013). These DS and OS populations were defined using stringent metrics for selectivity and all are statistically differentiable from each other, exhibiting normal distributions around a preferred direction or orientation of motion.

A comparison of populations of tectal cell and RGC input responses revealed emergent properties associated with local circuits of the zebrafish tectum. Specifically, the observation of a population of DS-PVNs tuned to RC (89 ± 11°, head-to-tail) motion which is conspicuously absent from the DS-RGC inputs. This emergent population is associated with an apparent functional remodeling of direction space from three equally spaced DS-RGC inputs into four cardinal tectal cell responses. In contrast to the transformation of direction space, we find that orientation space is represented similarly in both the RGC input and tectal cell populations, illustrating feature-dependent differences in how local tectal circuits process their retinal inputs: a direct readout of the retinal-world-view (OS) and a translation into a tectal world-view (DS).

Our study has used stringent inclusion criteria, culminating in relatively few cells per fish. Our empirical vector threshold translates to 92% of the identified DS cells having a Direction Selective Index (DSI) >0.5, compared with a DSI >0.3 for Gabriel et al. (2012) and DSI > 0.33 for Niell and Smith (2005). Indeed, compiling a large dataset of such highly DS cells has allowed us to reliably delineate populations of coherent responses. Previous studies (Niell and Smith, 2005; Gabriel et al., 2012) were unable to distinguish coherent populations, other than a preponderance of CR (anterior) motion selective cells. In contrast, we identify four cardinally arranged, statistically differentiable populations of DS-PVNs. Such discrepancies highlight the importance of undertaking large-scale studies with stringent criteria to determine coherent populations of responses and, in so doing, correctly characterize the computations of local circuits. Studies with insufficient power to clearly demonstrate or refute populations of responses will be susceptible to pooling of multiple populations into complex multivariate responses.

Recent studies have proposed contrasting models for the establishment of direction-selectivity in tectal cells. Grama and Engert (2012) provide evidence that direction-selectivity in the tectum may arise through convergence of nontuned excitatory inputs and inhibitory inputs that are tuned to the null direction. Alternatively, Gabriel et al., 2012 detail examples of DS tectal cells that receive excitatory and inhibitory inputs tuned to opposing directions. We find: (1) classes of DS tectal populations with preferred angles matching the DS input populations (suggestive of tuned excitatory inputs), and (2) additional DS tectal populations with preferred angles not present in the input populations (suggestive of tuning via an inhibitory mechanism within the tectal circuitry). Consequently, our findings demonstrate that Gabriel et al. (2012) and Grama and Engert (2012) are both cor-

rect and the apparent disparity between the two actually reflects the full repertoire of DS processing in the tectum (i.e., both retinal and tectal in origin). It will be interesting to characterize the DS mechanisms of the specific populations of DS tectal cells identified here. In particular, a functional dissection of the populations with preferred angles matching a DS input population compared with those with emergent properties may well reveal diverse mechanisms responsible for generating each functional phenotype.

In addition to the DS- and OS-PVN subtypes, we identify two populations of DS responses restricted to the superficial neuropil region of the tectum, and a number of OS cells that scatter across orientation space. One of the superficial DS populations (centered at 126°) represents another emergent population. Inhibitory cells within this spatially distinct region of the tectum have previously been characterized (Del Bene et al., 2010). These SINs were shown to be selective for large objects and play a role in size-based filtering of information from deeper tectal layers. Our findings extend the functional responsive range of these cells, suggesting that this cell type may be more functionally diverse than previously thought. Do they play a role in locally modulating circuits within the tectum based on the direction and orientation of stimulus motion?

Our key finding, the re-encoding of direction space, spotlights a conceptual challenge in our understanding of visual processing in vertebrates. Why does triangular arrangement of functional inputs morph into a cardinal one? What does this tell us about what the brain sees? Perhaps more importantly the emergent properties that we have identified provide a quantitative measure with which to probe the underlying circuits.

References

Ahrens MB, Orger MB, Robson DN, Li JM, Keller PJ (2013) Whole-brain functional imaging at cellular resolution using light-sheet microscopy. Nat Methods 10:413–420. CrossRef Medline

Batschelet E (1981) Circular statistics in biology. London; New York: Academic.

Ben Fredj N, Hammond S, Otsuna H, Chien CB, Burrone J, Meyer MP (2010) Synaptic activity and activity-dependent competition regulates axon arbor maturation, growth arrest, and territory in the retinotectal projection. J Neurosci 30:10939–10951. CrossRef Medline

Carandini M (2012) From circuits to behavior: a bridge too far? Nat Neurosci 15:507–509. CrossRef Medline

Del Bene F, Wyart C, Robles E, Tran A, Looger L, Scott EK, Isacoff EY, Baier H (2010) Filtering of visual information in the tectum by an identified neural circuit. Science 330:669–673. CrossRef Medline

Gabriel JP, Trivedi CA, Maurer CM, Ryu S, Bollmann JH (2012) Layer-specific targeting of direction-selective neurons in the zebrafish optic tectum. Neuron 76:1147–1160. CrossRef Medline

Grama A, Engert F (2012) Direction selectivity in the larval zebrafish tectum is mediated by asymmetric inhibition. Front Neural Circuits 6:59. CrossRef Medline

Hubel DH, Wiesel TN (1962) Receptive fields, binocular interaction and functional architecture in the cat's visual cortex. J Physiol 160:106–154. Medline

Lister JA, Robertson CP, Lepage T, Johnson SL, Raible DW (1999) nacre encodes a zebrafish microphthalmia-related protein that regulates neural-crest-derived pigment cell fate. Development 126:3757–3767. Medline

Lowe AS, Nikolaou N, Hunter PR, Thompson ID, Meyer MP (2013) A systems-based dissection of retinal inputs to the zebrafish tectum reveals different rules for different functional classes during development. J Neurosci 35:13946–13956.

Meyer MP, Smith SJ (2006) Evidence from in vivo imaging that synaptogenesis guides the growth and branching of axonal arbors by two distinct mechanisms. J Neurosci 26:3604–3614. CrossRef Medline

Niell CM, Smith SJ (2005) Functional imaging reveals rapid development of visual response properties in the zebrafish tectum. Neuron 45:941–951. CrossRef Medline

Niell CM, Stryker MP (2008) Highly selective receptive fields in mouse visual cortex. J Neurosci 28:7520–7536. CrossRef Medline

Niell CM, Meyer MP, Smith SJ (2004) In vivo imaging of synapse formation on a growing dendritic arbor. Nat Neurosci 7:254–260. CrossRef Medline

Nikolaou N, Lowe AS, Walker AS, Abbas F, Hunter PR, Thompson ID, Meyer MP (2012) Parametric functional maps of visual inputs to the tectum. Neuron 76:317–324. CrossRef Medline

Priebe NJ, Ferster D (2012) Mechanisms of neuronal computation in mammalian visual cortex. Neuron 75:194–208. CrossRef Medline

Swindale NV (1998) Orientation tuning curves: empirical description and estimation of parameters. Biol Cybern 78:45–56. CrossRef Medline